Kinetic Roughening in Molecular Beam Epitaxy of InP

M. A. Cotta
UNICAMP, IFGW/DFA, CP 6165, 13081 Campinas SP, Brazil

R. A. Hamm, S. N. G. Chu, R. Hull, L. R. Harriott,
AT&T Bell Laboratories, Murray Hill, NJ 07974, USA

and
H. Temkin
Colorado State University, Fort Collins, CO 80523, USA

Received July 21, 1995

An abrupt transition in the growth mode is observed for epitaxial films of InP prepared by metalorganic molecular beam epitaxy. Below a minimum growth temperature, T_g^{min}, three-dimensional growth and kinetically controlled roughening are observed, with surface roughness showing two distinc power law regimes dependent on film thickness. The observed roughening is attributed to the presence of a Schwoebel-Erlich-type barrier to adatom motion across surface steps. From the dependence of T_g^{min} on the substrate misorientation, we are able to estimate an upper limit of 0.4-0.5 eV for this barrier. At temperatures higher than T_g^{min}, we observe smooth morphologies with the concurrent formation of localized defects associated with P-vacancies. The density of defects is strongly dependent on the thermodynamic and kinetic growth parameters.

I. Introduction

Molecular beam epitaxy (MBE) is an important deposition process and there is considerable interest, experimental as well as theoretical, in achieving detailed understanding of surface morphology of epitaxial layers and the underlying kinetic phenomena. The growth mechanism usually depends on surface diffusion of atoms to kink sites, which are energetically more favorable to nucleation. The morphology of the epitaxial film is then influenced by deposition rate, which controls the adatom population on the surface, and substrate temperature, which affects the surface diffusion rate of the species. There are thus different forms of kinetic roughening, depending on the relative magnitude of these variables. In particular, at low temperatures the reduced surface mobility can lead to three-dimensional growth, where islands nucleate on incomplete monolayers. At low growth temperatures surface roughness and a transition to three- dimensional (3D) growth can arise also as a result of a potential barrier to surface diffusion. Schwoebel[1] and Erlich (SE)[2,3] proposed the existence of such a barrier at step edges, which results in adatoms already on the terrace having a higher probability of staying on top than moving down.

Recently, there has been considerable theoretical interest in surface roughness and growing interfaces. In particular, scaling behavior of the interface width - or surface roughness, $W \equiv [< (h- < h >)^2 >]^{1/2}$, where h is the film thickness - is observed in these models. The scaling is expected to be of the form:

$$W(L,t) \sim L^{\alpha} f(t/L^{\alpha\beta})$$

where $f(x) \sim x^{\beta}$ for $x << 1$ and $f(x) \rightarrow$ const for $x >> 1$, for a system with size L and time t[4,5]. The constants α and β are known as the roughness and growth exponents, respectively. A number of models have been proposed to describe the growing interface in detail[4-8].

Several experiments have been performed to understand the processes controlling semiconductor MBE growth. Scanning tunneling microscopy of submonolayer growth of Si on Si(100) has shown that surface diffusion is highly anisotropic[9,10]. The existence of a limiting thickness beyond which the film is not epitaxial, with a growth rate-dependent activation energy, was observed by transmission electron microscopy (TEM) of Si MBE on Si(100)[11]. From the theoretical point of view, simulations based on the solid-on-solid model[12] showed that the thermally activated nature of surface diffusion determines the limiting thickness and its strong temperature dependence. W was postulated to build gradually with film thickness up to a saturation value, implying a continuous transition from smooth to rough surfaces. A different model, proposed by Kessler *et al.*[13], considered ballistic aggregation as the sticking mechanism and surface diffusion (BASD) during MBE growth. Simulations for $d = 2$ dimension, for varying diffusion lengths, show a fairly abrupt transition between two power law regimes for the dependence of W on h. The first represents surface diffusion scaling, and the second, along with the subsequent saturation, is described by the Kardar-Parisi-Zhang equation[7]. In addition the first power law regime, for short growth times, is characterized by an exponent $\beta \sim 0.25$, significantly lower than that predicted by other authors[14,15]. The measured growth exponents reported in literature[9−11], however, do not allow for discrimination between models.

In this work we discuss changes in surface morphology of InP grown by metalorganic MBE (MOMBE). Using scanning force microscopy we observe a discontinuous build-up of roughness with film thickness. We observe a transition between two power-law regimes for the roughness dependence on film thickness, as predicted by Kessler *et al.*[13]. This transition leads to the formation of elongated multi-terrace structures, running along the $[0\bar{1}1]$ direction as an intermediate step towards a grain-like surface[16]. We also show that the kinetically controlled roughening occurs below a minimum growth temperature, T_g^{min}, which also marks the transition to 3D growth. This temperature depends strongly on group III and V fluxes and the misorientation of the substrate used. From the roughening dependence on temperature, for different substrate misorientations, we are able to estimate the maximum value of the Schwoebel-Erlich barrier to be 0.4-0.5 eV. At temperatures higher than T_g^{min} smooth morphologies and flat interfaces are obtained for all thicknesses. The roughness values in these samples are always smaller than for samples grown below T_g^{min} independent of the film thickness. In the growth above T_g^{min}, however, we also observe two types of surface defects, which we call oval and small defects. The density of oval defects present in the InP layers grown by MOMBE is completely independent of the growth parameters, the defects being entirely attributed to surface contamination of the substrate. Such defects are discussed elsewhere[17]. The small defect density depends on the growth conditions and substrate misorientation. This indicates that defect formation is most likely related to re-evaporation of P and the localized P-deficiencies in the film occurring under conditions where surface diffusion is the dominant relaxation mechanism.

II. Experimental

The homoepitaxial layers were grown on nominally (100)-oriented InP substrates with misorientations of 0.08, 0.12 and 0.23°. Substrates miscut by 1.5° off (100), towards the < 111 >A direction, and by 2° off towards the < 111 >B direction were also used. The films were grown in a MOMBE chamber using trimethylindium (TMI) and triethylgallium (TEG) as group III sources. Phosphine (PH_3) passing through a low-pressure cracking cell provided exclusively P_2 as the group V precursor. The substrate temperature was varied in the range 480 to 525°C and measured by a thermocouple immersed in In in a hole at the back of the sample holder, assuring excellent temperature control and reproducibility[18]. Before growth, the substrate was heat treated to 550°C for about 20 seconds under a P_2 flux and rapidly returned to the growth temperature. In-air atomic force microscope (AFM) with high aspect ratio (3:1) Si tips was used for the roughness measurements.The rms roughness of these heat-treated surfaces was $W \sim 0.3-0.5$Å. The rms roughness of the initial substrate was $W \sim 0.5$Å. Subsequent annealing of the grown samples at growth temperature, under P_2 flux, did not change the surface morphology. Normarski and transmission electron microscopies (TEM)

were also used.

MOMBE, unlike elemental source MBE, involves chemical reactions and catalysis of species on the surface during growth. In MOMBE, the growth rate R depends on temperature, due to changes in the cracking of metalorganics on the surface or evaporation of species[19]. However, the range of temperatures used in this study provided R constant with temperature for each set of group III and V fluxes used. This is the region where MOMBE most closely resembles MBE.

III. Results and discussion

Fig. 1 shows the surface morphologies of 300nm-thick films grown with different growth rates R. The roughness increases with R and the surface evolves from a smooth, two-dimensional growth to a pattern with elongated multi-terrace structures with a period of $\approx 0.1 - 0.15\mu$m running along the $[0\bar{1}1]$ direction. We can observe that the sample grown with higher growth rate shows a smaller height variation though the structures are more irregular. This corresponds to the filling up of the valleys between the multi-terraces at the same time that the multi-terraces themselves get more irregular. The surface evolves eventually to structures in form of grains resulting from the irregularities on the multi- terraces formed along the $[0\bar{1}1]$ direction. The formation of such periodic structures for larger values of R is also observed in the TEM of InP films grown with InGaAs marker layers (Fig.2). This multilevel system of terraces agrees in depth and profile with the cross section of the AFM pictures. We thus believe that tip convolution effects in the narrow trenches are negligible. This kind of morphology could be expected if any anisotropy along the two perpendicular crystallographic directions is reflected in the rates of the kinetic processes taking place on the surface during growth.

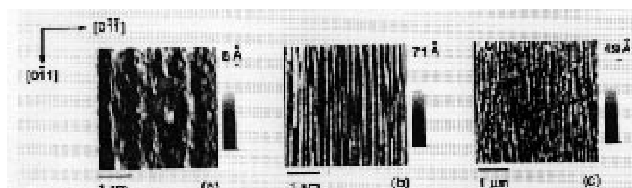

Figure 1. $4 \times 4\mu m^2$ AFM pictures of 300nm-thick films grown with R: (a) 1.4 Å/s; (b) 2.2 Å/s and (c) 4.6 Å/s (T=505°C), determined by varying the TMI flux. The gray scale indicates the height variation in the figure.

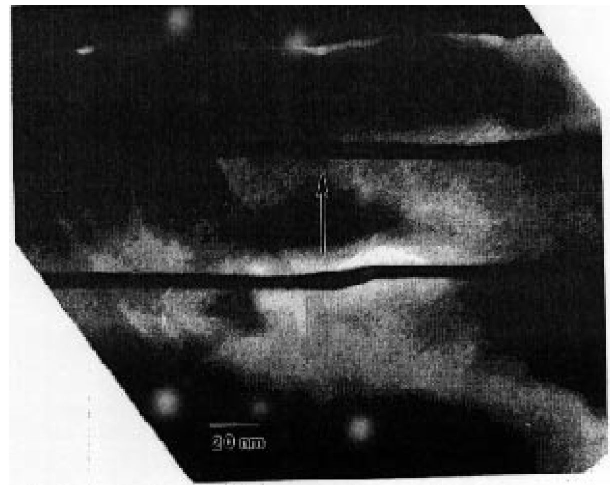

Figure 2. $[0\bar{1}1]$ cross section TEM of InP film with elongated structures along the $[0\bar{1}1]$ direction, grown with InGaAs marking layers (dark).

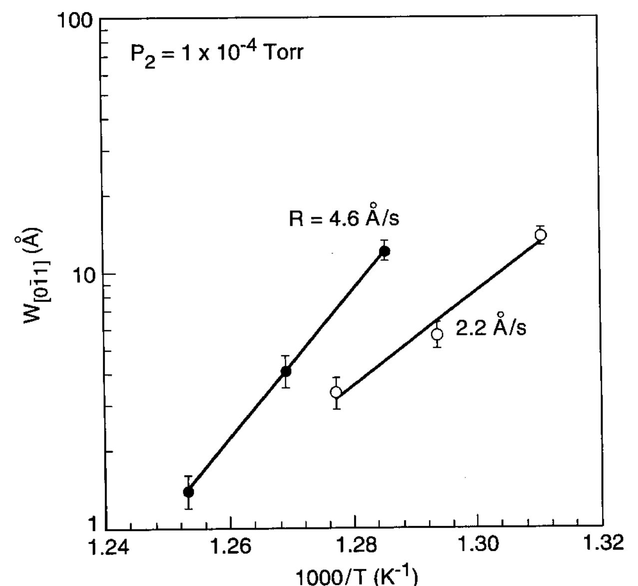

Figure 3. Temperature dependence of rms roughness W along the $[0\bar{1}1]$ direction, for different R. W was measured on 1-2 μm long cross sections of the surface.

We have observed that increasing P_2 flux, and or R, increases W. These changes result in less time for the molecules to migrate on the surface[20], and indicate that the diffusion process is in the origin of the different morphologies observed. Ghaisas and das Sarma[21] have shown that the diffusion length depends on the ratio of deposition rate (here the growth rate R, since R is constant with temperature) to atomic hopping rate at the growth front. The shapes observed in Fig. 1 would then come from anisotropic diffusion of the In species along the two crystallographic directions.

With regard to the elongated structures, their formation is likely related to faceting, which can be observed in the TEM (Fig. 2) of our samples. The development of different facets near crystal edges is commonly observed in the epitaxy on patterned substrates. In fact, high resolution cross section TEM of the elongated multi-terraces show a facet with an angle of 19 ± 1^0, indicating that $\{411\}$ planes are forming on these samples as well, and that energetics is also playing a role in determining the growth front and morphology.

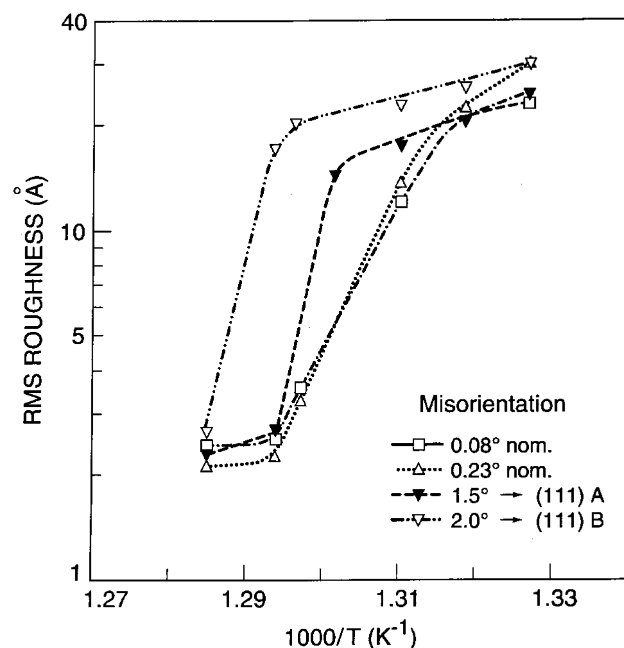

Figure 4. Variation of surface roughness W with growth temperature for substrates with different misorientations. All films used here were 300nm thick (scan size $4 \times 4\mu m^2$).

If a kinetic process like anisotropic diffusion is involved in the surface roughening, we expect to see similar changes when the temperature is varied. Fig. 3 shows the variation of W along the $[0\bar{1}1]$ direction with growth temperature for 300nm-thick InP films. We see in Fig. 3 that W depends exponentially on temperature, increases more rapidly for samples grown with higher growth rates, and gets to the values observed at planar surfaces at finite growth temperatures. The latter points to the existence of a minimum growth temperature T_g^{min}, for each set of growth parameters, above which 2D growth begins to take place and below which 3D growth occurs.

Fig. 4 plots W (for 300nm-thick InP films grown at a constant growth rate R) as a function of growth temperature for different substrate misorientations. For the higher temperatures used, the surface is smooth, characteristic of two-dimensional (2D) growth. As the temperature drops below $\approx 500°C$ there is a rapid increase in roughness, corresponding to the formation and disappearance of the elongated multiterraces, eventually leading to a grain-like surface. The transition is more abrupt in the case of the misoriented substrates, and occurs at a temperature 5-10°C higher than for the nominal substrates. In this sense the minimum growth temperature, T_g^{min}, even though not exactly determined, is substrate dependent. This value is close to 505°C for the misoriented substrates and lower than 500°C for the nominal surfaces. We can also observe that the rate of increase of W with the drop in temperature is different for the vicinal surfaces and so is the activation energy for roughening.

The data of Fig. 4 shows that T_g^{min}, is lower for substrates with lower misorientation angles. This is consistent with the idea of a SE-type barrier playing an important role in the roughening process. The presence of such a barrier would result in lower effective diffusion rates for atoms close to the step edges being formed on the growing surface; atoms far from edges would not be affected. At growth conditions resulting in rapid surface diffusion the increase in adatom residence time at sites close to step edges should be negligible; the mobility insured by large hopping rate values (or by larger time intervals between adsorption and incorporation) will provide the adatoms a finite probability of overcoming the energy barrier or moving away from them before being incorporated. Under these conditions the difference in diffusion at different regions of the surface would be negligibly small. On the other hand, changes in the hopping rate[22,23] with temperature are proportional to the energy barrier for surface diffusion; variations in growth temperature have a proportionally larger effect on hopping rates of less mobile adatoms. In this sense, at lower growth temperatures, the presence of a SE-type barrier would increase the incorporation probability in the sites close to step edges, resulting in islands growing faster in the region close to these sites. Eventually this process of adatom pinning at the top of terrace edges could be interpreted as localized differences in growth rate along the surface, leading to the formation of elongated structures. The shape of these structures should reflect the anisotropy of adatom diffusion rates. This departure from a planar surface will then lead to the formation of crystallographic planes other than (100) and to the faceting observed in our samples.

The region of Fig. 4 in which significant differences exist in diffusion along the surface corresponds to the regime of rapid increase in W with the drop in temperature. The roughening process commences at a temperature T_g^{min} at which these differences reach a critical value. Once a morphology characterized by grain-like structures is reached, however, the average barrier to diffusion all over the surface will be roughly the same and the local differences in diffusion are no longer important. This results in a slower increase in W with the drop in temperature as observed in Fig. 4. In the low temperature limit of Fig. 4 this region exhibits smaller activation energy clearly visible in the case of vicinal surfaces. The values obtained in this case are in the range 1.0-1.5eV, close to others reported in literature for roughening associated to 3D growth[11].

We thus postulate that the difference in local diffusion rates associated with the presence of SE barriers at the step edges is the main cause for the different roughness regimes shown in Fig. 4. We assume that roughening associated to 3D growth will eventually occur with an activation energy E_f for an initially flat substrate due to step edges formed during nucleation at sufficiently low growth temperatures and that an initial density of barriers will only accelerate the process. The initial density of barriers would then be responsible for the unphysically large activation energies associated to the fast roughening, for instance $E_{0.08} = 7.6$eV for the 0.08° substrate. We can obtain an estimate of the magnitude of this barrier if we write the activation energy for the 2D-3D growth mode transition as

$$E_{at} = E_f + \mathbf{n}_f \cdot E_{SE}$$

where E_{at} is the activation energy for the transition region for a given set of the growth parameters, E_{SE} is the SE-barrier and $\mathbf{n}_f$ is a factor representing the density of barriers normalized to that of a nominal surface[24]. This factor reflects the initial barrier density at the surface if we assume that the terraces are nucleated independently of each other, i.e. the number of step edges being formed at each terrace is independent of the terrace width, and that the barriers are isotropic, i.e. independent of the type of step present at the surface. Such assumptions apply in the initial stages of the roughening process on vicinal surfaces. Using the lowest miscut surfaces as a reference we can write

$$E_{at} = E_{0.08} + \mathbf{n}_f^{0.08} \cdot E_{SE}$$

where $E_{0.08}$ is the activation energy for the substrate with 0.08° miscut and $\mathbf{n}_f^{0.08}$ is the step density factor. Since we are normalizing to the 0.08 substrate the step density factor can be written as the ratio of the step densities (given by the misorientation angles) of the substrates. Assuming an exponential activation of roughness with the growth temperature in the 5°C interval where the growth mode transition for vicinal substrates takes place, we obtain an estimate of 0.4 - 0.5eV for the SE barrier from all three curves (0.23, 1.5 and 2° substrates) in Fig. 4.

The values obtained for E_{SE} are large, of the order of two surface bond energies, but are consistent with the idea of a barrier responsible for the rapid roughening process observed. This estimate actually represents the maximum value for the energy barrier; contributions from step edges formed subsequently during growth are neglected. In fact, a 0.2eV barrier at step edges was introduced in Monte Carlo simulations in order to reproduce reflection high energy electron diffraction intensity oscillations observed during GaAs growth[25].

The elongated multiterraces imaged by AFM on 2° off substrate are aligned at an angle of $\approx 45°$ to the $[0\bar{1}1]$ direction, differently from the nominal and 1.5° off substrates. The low miscut nominal substrates present low step density, with no preferential step direction. For the 1.5° off substrate steps run along the [011] direction so that diffusion along the $[0\bar{1}\bar{1}]$ direction is inhibited. Since diffusion is already slower in this direction[19,20], the presence of A steps should facilitate the roughening process. For the 2° off substrates, however, B steps run along the $[0\bar{1}\bar{1}]$ direction, and diffusion along $[0\bar{1}1]$ direction is inhibited. In this sense, the presence of B-steps causes a larger shift in T_g^{min} than A-steps. In GaAs the A-steps are known to be smooth while the B-steps are kinked and more reactive[26]. If the same is true for InP, the presence of B-steps would compensate for the surface anisotropy and inhibit the formation of the elongated structures. However, since kinks in B-steps are A-steps, this supression may not be complete. The high density of A-steps in the 2° off substrate results in multiterraces shorter and less regular than those occuring on nominal surfaces. The alignment direction is given by the terrace width and the consequent interaction of A steps along different terraces. We observed that the alignment direction indeed depends on the misorientation angle. The overall shape and period of the elongated multiterraces on the vicinal surfaces, though, is still close to those observed in nominal substrates.

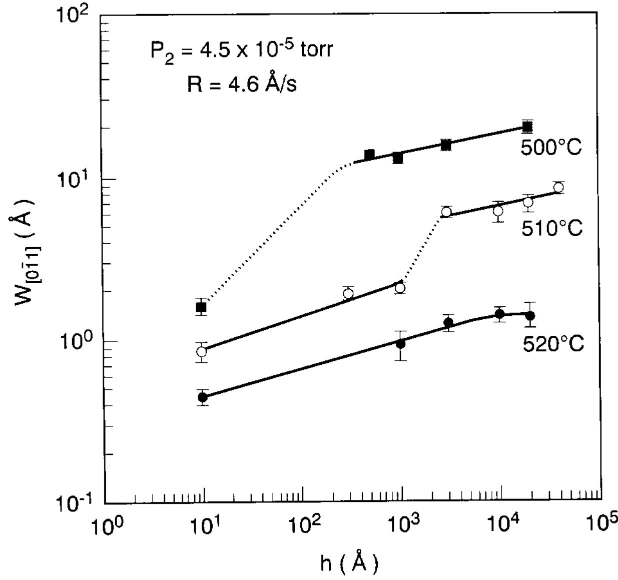

Figure 5. Dependence of rms roughness W along the $[0\bar{1}1]$ direction on the film thickness h as a function of growth temperature. W was measured on 1-2 μm long cross sections of the surface.

When varying only the film thickness, at temperatures lower than T_g^{min}, we observe an evolution of surface roughness, with the same morphologies shown in Fig. 1. A smooth surface evolves into a pattern with elongated terraces aligned in the $[0\bar{1}1]$ direction. As thickness increases, roughness also builds up along the $[0\bar{1}1]$ direction, leading eventually to surfaces with isotropic, grain-like structures. Fig. 5 shows the roughness W as a function of the film thickness for samples grown at different temperatures and the same growth rate. We observe that at 520°C W increases slowly with thickness, and seems to saturate when $h \sim 1-2\mu$m. At 510°C, there is a sudden increase of W with h between 100 and 300 nm, but for h values below or above this interval, power-law regimes can be observed. At 500°C, the roughness builds up very rapidly at the beginning of the growth, the surface showing grain-like structures, but a power-law regime again sets in for films thicker than 30 nm, with an exponent ($\beta \sim 0.1$) close to that observed for $h \sim 300$nm at 510°C.

Fig. 5 provides the opportunity of comparing our experimental results with the BASD model. Kessler *et al.*[13] calculated the interface width W as a function of film thickness for varying lengths of a diffusion step. Since surface diffusion, and the corresponding diffusion length, increase with substrate temperature, a qualitative comparison between theory and the experimental data on Fig. 5 seems appropriate. We can then see that the predicted transition between two-power law regimes[13] is clearly observed in our samples. Also, the length of the first power-law regime increases with growth temperature and, consequently, with the diffusion length. The power-law exponent observed for the samples grown at 520°C and at 510°C, in the range $h \sim 1-100$ nm, is $\beta \sim 0.2$, close to the value predicted by the BASD model[13]. It is interesting to notice, however, that aggregation models like the BASD are not considered the most adequate to describe epitaxy by MBE techniques at usual growth temperatures. We believe that the agreement between our results and those from the theoretical model are due to the more physical surface diffusion used by Kessler *et al.*[13], which may have played a similar role to that of a SE-like barrier on their calculation.

We would like to stress that our results are very different from the limiting thickness for an amorphous-crystalline transition observed by Eaglesham *et al.*[11] for low temperature Si MBE. Although we observe roughness characteristic of three-dimensional growth, the material obtained is of good crystal quality. No significant difference is observed in the bulk electrical or optical properties of InP films grown with different morphologies.

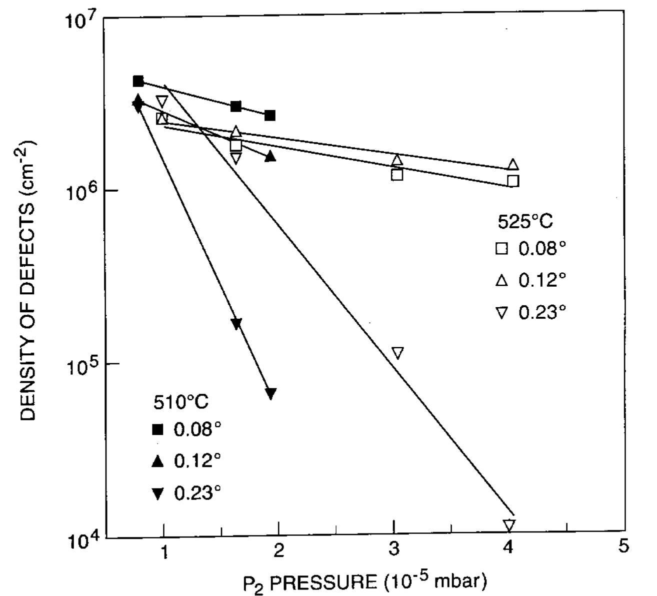

Figure 6. Density of defects as a function of P_2 pressure for different substrate misorientations at two growth temperatures (510 and 525°C).

When growth conditions ($T_g > T_g^{min}$) result in smooth InP morphologies, we observe the concurrent formation of defects on the surface; the morphology of the surface in between them, however, is flat and characteristic of 2D growth. The defect density is strongly

related to the thermodynamic growth parameters, P_2 pressure and temperature, and the miscut which controls surface kinetic conditions. Fig. 6 shows the density of defects as a function of the P_2 pressure used in the growth on slightly miscut substrates, at two different growth temperatures, 510 and 525°C. No such defects were observed in the substrate with 2° misorientation, under any growth conditions; the 1.5° off substrate was not used for these measurements. For P_2 pressures larger than $\approx 2 \times 10^{-5}$mbar roughening (and no defects) is observed for samples grown at 510°C. The defect density grows exponentially with the decrease in P_2 pressure. The defect formation rate varies with miscut and temperature. It is essentially the same for the 0.08 and 0.12° substrates, at both temperatures, and has a larger value for the substrate with 0.23° miscut. At the higher temperature the formation rates decrease for all substrates and the differences between substrates become smaller.

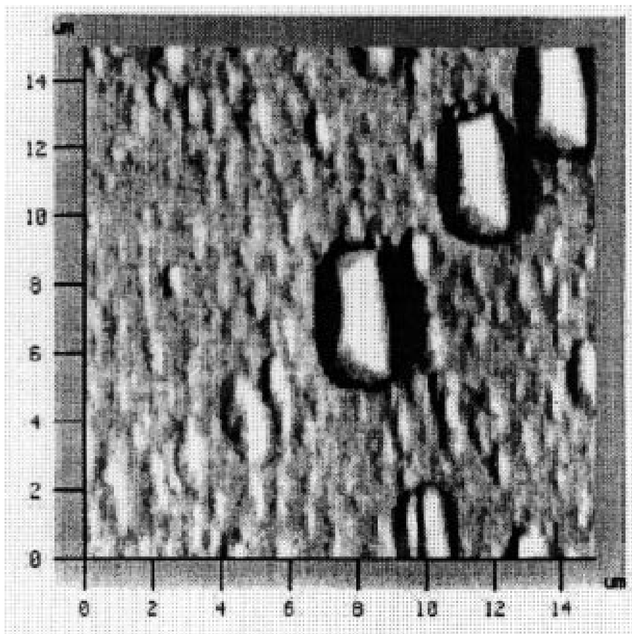

Figure 7. AFM picture ($15 \times 15\mu m^2$ scan size) of InP surface grown at 525°C under a P_2 flux of $\approx 1 \times 10^{-5}$mbar showing the presence of small defects in between the oval (large) defects.

Fig. 7 shows an AFM picture of an InP surface grown at 525°C under a P_2 flux of $\approx 1 \times 10^{-5}$mbar. At higher P_2 fluxes and lower temperatures the density of defects is smaller, consistent with the data of Fig. 6. The angles observed on the sidewalls of these defects are very shallow ($\approx$ 1-2°) with the higher values observed in cross sections along the $[0\bar{1}1]$ direction. The ratio between the lengths along the two major crystallographic axis is $\approx$ 2- 3. This ratio reflects the anisotropy of the surface diffusion rates which are highest along the $[0\bar{1}1]$ direction[27,28]. The shallow angles indicate there is no faceting involved in the growth of these features. The dislocation densities of the substrates used here ($< 5 \times 10^3 cm^{-2}$) are well below the defect densities observed in the samples. In addition, for growth rates above a critical value the defect density increases linearly with the growth rate. This points to the existence of a critical V/III ratio below which the defect density begins to increase. Above this critical value, the defects disappear. The absence of defects in the 2° off substrate gives support to this hypothesis. The defects are never observed in the rough surfaces clearly demonstrating that the defects are the macroscopic response to a perturbation in the surface during 2D growth. These results point to a connection between the formation of defects and the P incorporation in the growing film. The loss of P from the surface through low incorporation or high evaporation would be inhibited in substrates with higher miscut, due to the higher density of nucleation sites. This, and the observed dependence on the growth conditions, indicate that the defects are likely related to group V vacancies. The high vapor pressure of P in InP and the resulting high re-evaporation rate at high temperatures make such a process quite likely[29]. Transmission electron microscopy shows the absence of dislocations or polycrystalline cores in defects like those shown in Fig. 7. However, if growth conditions allow these defects to grow in size dislocation loops form inside the defect region[14], suggesting their origin as the condensation of point defects like P-vacancies.

It is interesting to note that these defects are very similar in shape to the mounded structures attributed to the growth instability on nominal GaAs substrates[30]. In addition, the oval defects resulting from surface contamination and commonly observed in epitaxy of GaAs and InP[31−34] also present the same shape (angle and length ratios), though with much larger sizes. Apparently the growing surface relaxes in the same way whether a local perturbation in the 2D growth is introduced by intrinsic (P-defficiency) or extrinsic (contamination) factors.

In summary, we investigate the temperature dependence of a 2D-3D transition in the MBE growth of homoepitaxial layers of InP. The morphology of InP presents two distinct regions. Below a minimum growth temperature T_g^{min}, 3D growth and kinetically controlled roughening attributed to the existence of a

Schwoebel-Erlich-type barrier occur. From the dependence of T_g^{min} on the substrate misorientation we obtain a maximum estimate of ≈0.4-0.5eV for this barrier. The dependence of roughness on film thickness shows two power-law regimes in agreement with the BASD model of Kessler *et al.*[13]. At temperatures higher than T_g^{min}, smooth surface morphologies are observed with the simultaneous formation of defects. The density of defects observed at high temperatures and low V/III ratios increases with a rate that depends on the substrate misorientation. These defects are thus affected by a combination of thermodynamic and kinetic factors, their microscopic origin being related to P-vacancies on the growing surface.

Acknowledgments

One of the authors (MAC) acknowledges financial support from CAPES and CNPq (Brazil). The research at CSU is supported by ONR under grant N00014-94-0003.

References

1. R. L. Schwoebel and E. J. Shipsey, J. Appl. Phys. **37**, 3682 (1966).
2. G. Erlich and F. G. Hudda, J. Chem. Phys. **44**, 1039 (1966).
3. H. W. Fink and G. Erlich, Surf. Sci. **143**, 125 (1984).
4. J. G. Amar and F. Family, Phys. Rev. A **41**, 3399 (1990).
5. F. Family and T. Vicsek, J. Phys. A**18**, L75 (1985).
6. J. Kertész and D. E. Wolf, J. Phys. A **21**, 747 (1988).
7. M. Kardar, G. Parisi and Y. Zhang, Phys. Rev. Lett. **56**, 889 (1986).
8. J. Chevrier, V. LeThanh, R. Buys and J. Derrien, Europhys. Lett. **16**, 732 (1991).
9. Y.-W. Mo, B. S. Swartzentruber, R. Kariotis, M. B. Webb and M. G. Lagally, Phys. Rev. Lett. **63**, 2393 (1989)
10. Y.-W. Mo, J. Kleiner, M. B. Webb and M. G. Lagally, Phys. Rev. Lett. **66**, 1998 (1991).
11. D. J. Eaglesham, H.-J. Gossman and M. Cerullo, Phys. Rev. Lett. **65**, 1227 (1990).
12. S. das Sarma and P. I. Tamborenea, Phys. Rev.B **46**, 1925 (1992).
13. D. A. Kessler, H. Levine and L. M. Sander, Phys. Rev. Lett. **69**, 100 (1992).
14. S. das Sarma and P. Tamborenea, Phys. Rev. Lett. **66**, 325 (1991).
15. D. Wolf and J. Villain, Europhys. Lett. **13,** 389 (1990).
16. M. A. Cotta, R. A. Hamm, T. W. Staley, S. N. G. Chu, L. R. Harriott, M. B. Panish and H. Temkin, Appl. Phys. Lett. **70**, 4106 (1993).
17. M. A. Cotta, R. A. Hamm, S. N. G. Chu, L. R. Harriott and H. Temkin, Appl. Phys. Lett. **66**, (1995).
18. R. A. Hamm, D. Ritter, H. Temkin, M. B. Panish, J. M. Vandenberg and R. D. Yadvish, Appl. Phys. Lett. **59**, 1893 (1991).
19. J. Ch. Garcia, Ph. Maurel, Ph. Bove and J. P. Hirtz, J. Appl. Phys. **69**, 3297 (1991).
20. M. Hata, A. Watanabe and T. Isu, J. Cryst. Growth **111**, 83 (1991).
21. S. V. Ghaisas and S. Das Sarma, Phys. Rev.B **46**, 7308 (1992).
22. J. H. Neave, P. J. Dobson, B. A. Joyce and J. Zhang, Appl. Phys. Lett. **47**, 100 (1985).
23. T. Shitara, D. D. Vvedensky, M. R. Wilby, J. Zhang, J. H. Neave and B. A. Joyce, Phys. Rev. B **46**, 6825 (1992).
24. J. Y. Tsao, *Materials Fundamentals of Molecular Beam Epitaxy* (Academic Press, Boston, 1993), p.211.
25. B. A. Joyce, communication in *Critical Issues in Epitaxy* Workshop, Boulder, CO, USA, June 24-26, 1994.
26. M. D. Pashley, K. W. Haberern and J. M. Gaines, Appl. Phys. Lett. **58**, 406 (1991).
27. K. Ohta, T. Kojima and T. Nakagawa, J. Cryst. Growth **95**, 71 (1989).
28. T. Ohno, K. Shiraishi and T. Ito, 1993 Materials Research Society Fall Meeting, Boston, MA, USA, Symp.
29. -M. B., Panish and H. Temkin, *Gas Source Molecular Beam Epitaxy*, (Springer Verlag, Berlin, 1993), p. 23-24.
30. M. D. Johnson, C. Orme, A. W. Hunt, D. Graff, J. Sudijono, L. M. Sander and B. G. Orr, Phys. Rev. Lett. **72**, 116 (1994).
31. N. Chand and S. N. G. Chu, J. Cryst. Growth **104**, 485 (1990).
32. P. K. Khulbe, P. S. Dobal, H. D. Bist, S. K. Mehta, R. Muralidharan and R. K. Jain, Appl. Phys. Lett. **63**, 488 (1993).
33. M. Lambert, A. Pèralés, R. Vergnaud and C. Stark, J. Cryst. Growth **105**, 97 (1990).
34. Y. Morishita, S. Maruno, M. Gotoda, Y. Nomura and H. Ogata, J. Cryst. Growth **95**, 176 (1989).